Ch 11
Particulate suspensions

Issues

Stability (dispersion)
sedimentation
migration
wall slip

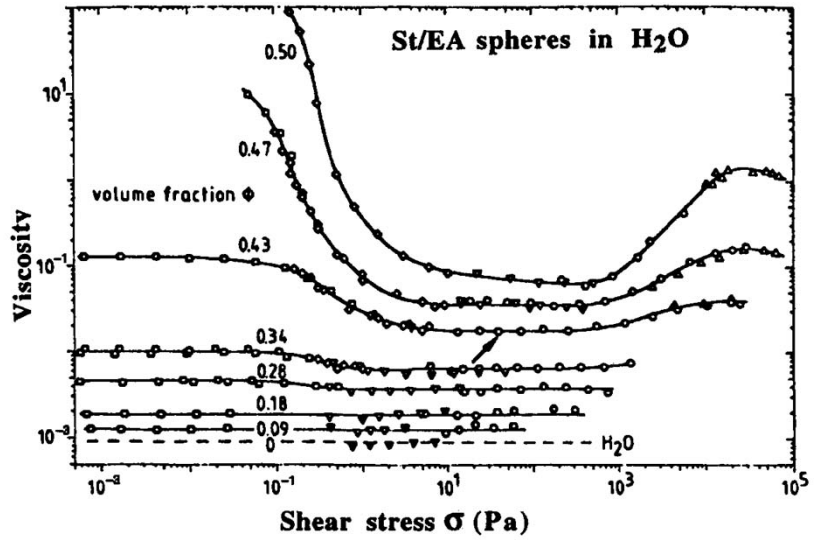

Figure 6.1 Viscosity versus shear stress for aqueous suspensions of charged poly(styrene-ethylacrylate) copolymer spheres of diameter $d = 250$ nm at various volume fractions ϕ and $T = 25°C$. The NaOH concentration was varied with ϕ over the range 0.022–0.230 M to keep the pH in the range 6.2–6.5. (From Laun 1984a, reprinted with permission from Hühig & Wepf Verlag.)

Hard spheres

Only rigid repulsions present when particles come into contact

Zero shear viscosity

$$\eta = \eta_s(1+2.5\phi)$$

$$\eta_r \equiv \frac{\eta}{\eta_s} = 1+2.5\phi+6.2\phi^2$$

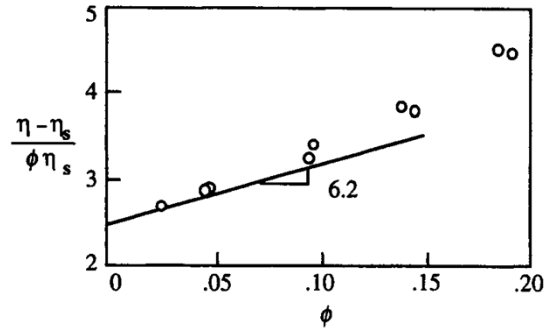

Figure 6.2 Reduced viscosity of suspensions of sterically stabilized polystyrene "hard spheres" of diameter $d = 420$ and 870 nm, as a function of volume fraction ϕ, replotted from data of Saunders (1961), compared to the prediction of Eq. (6-2). (From Macosko, *Rheology Principles, Measurements, and Applications*, Copyright © 1994. Reprinted by permission from John Wiley & Sons.)

$$d\eta = 2.5\eta(\phi)d\phi \qquad \eta = \eta_s \exp(5\phi/2) \qquad \eta = \eta_s \exp([\eta]\phi) \qquad [\eta] = \lim_{\phi\to 0}\frac{\eta-\eta_s}{\phi\eta_s}$$

$$\eta = \eta_s\left(1-\frac{\phi}{\phi_m}\right)^{-[\eta]\phi_m}$$

Krieger-Dougherty equation

Hard spheres

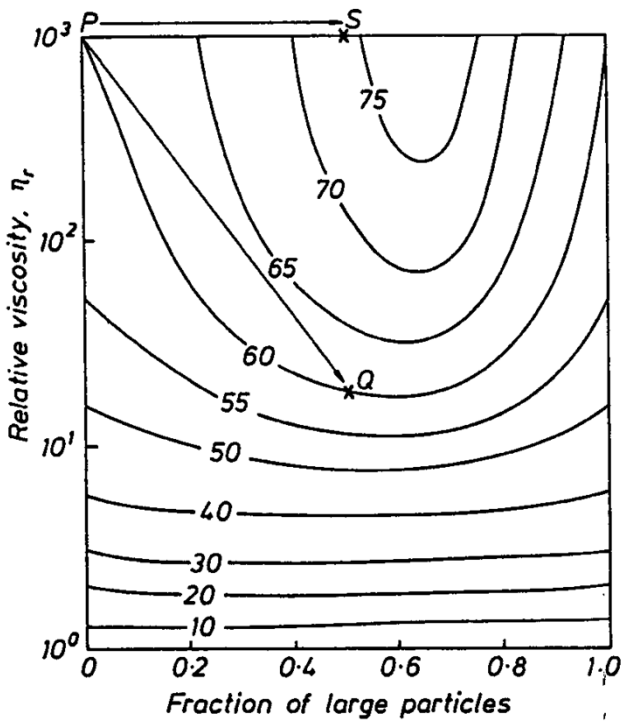

Figure 6.3 Relative viscosity as a function of the fraction of large spheres in a bimodal distribution of particle sizes with a 5:1 ratio of diameters, at various total volume percentages of particles. The arrow $P \rightarrow Q$ illustrates the 50-fold reduction in viscosity that occurs when monosized particles in a 60 vol% suspension are replaced by a 50–50 mixture of large and small spheres. The arrow $P \rightarrow S$ shows that if monosized spheres are replaced by a bimodal size distribution, the concentration of spheres can be increased from 60% to 75% without increasing the viscosity. (Reprinted from Barnes et al., *An Introduction to Rheology* (1989), with kind permission from Elsevier Science - NL, Sara Burgerhartstraat 25, 1055 KV Amsterdam, The Netherlands.)

Viscosity can be reduced when particles of different sizes are mixted
Higher volume fractions of particles can be packed into a suspension
Of practical importance in the formulation of highly loaded suspension
-> allows thermal expansion coefficient be closely matched to the devices
-> prevent crack and debonding

Hard spheres

Shear thinning

$$D_0 = \frac{k_B T}{6\pi\eta_s a} \qquad t_D \approx \frac{a^2}{D_0} = \frac{6\pi\eta_s a^3}{k_B T}$$

time for a particle to diffuse a distance equal to its radius

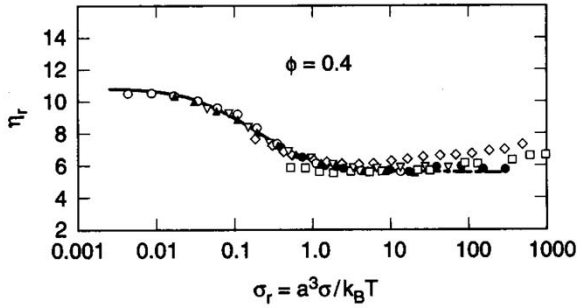

Figure 6.4 Relative viscosity $\eta_r \equiv \eta/\eta_s$ verses reduced shear stress for latices of poly(methylmethacrylate) spheres of radii 85, 141, 204, and 310 nm, sterically stabilized by adsorbed triblock copolymer, poly(dimethylsiloxane)–polystyrene–poly(dimethylsiloxane), in silicone fluids of viscosity 7.98 cP and 44.1 cP at 30°C. The line is the fit from Eq. (6-14a). (From Choi and Krieger 1986, reprinted with permission from Academic Press.)

$$Pe \equiv \frac{\eta_s \dot{\gamma} a^3}{k_B T} \propto \dot{\gamma} t_D$$

$$\sigma_r \equiv \frac{\sigma a^3}{k_B T}$$

$$\frac{\eta - \eta_\infty}{\eta_0 - \eta_\infty} = \frac{1}{1 + \sigma/\sigma_c}$$

Universal function of Pecle number for fixed volume fraction

Hard spheres

Mechanism of shear thinning & shear thickening

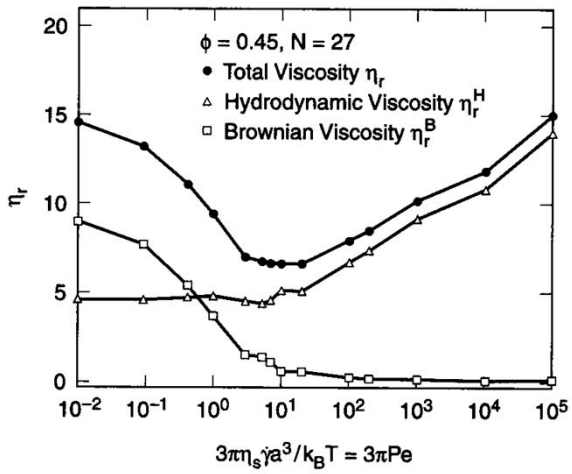

Figure 6.8 Stokesian dynamics simulation results for the steady shear viscosity at $\phi = 0.45$; also shown are the separate contributions of the Brownian and hydrodynamic stresses. (From Phung et al. 1996, with peremission from Cambridge University Press.)

Shear thinning;
1.disappearance of Brownian contribution
-> viscosity reduction by a factor of 2
2.formation of lines of particles (strings) parallel to the flow direction
-> evidenced by computer simulation & light scattering

Shear thickening;
1.formation of clusters containing particles driven by shear into close proximity
2.deformation of clusters produces large lubrication stresses in the thin films separating closely spaced particles
3.the mechanism depends on the nature of the repulsive potential

Non-spherical particles

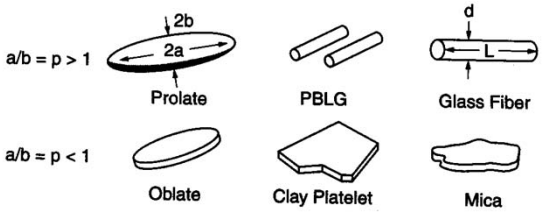

Figure 6.13 Prolate and oblate shapes of various particles. (Adapted from Macosko, *Rheology Principles, Measurements, and Applications*, Copyright © 1994. Reprinted by permission from John Wiley & Sons.)

Dilute suspensions

Jeffery orbits

In the absence of Brownian motion and of interparticle interactions,

$$\dot{\mathbf{u}} = \mathbf{u}\cdot\boldsymbol{\omega} + \left(\frac{p^2-1}{p^2+1}\right)(\mathbf{u}\cdot\mathbf{D} - \mathbf{uuu}:\mathbf{D})$$

In a shearing flow, $\tan\theta = p\tan\left(\frac{\dot{\gamma}t}{p+1/p}\right) + \tan\theta_0$

θ; the angle of the axis of symmetry measured in the clockwise direction from the flow direction

θ is time-periodic; a non-Brownian axisymmetric particle rotates indefinitely in a shear flow with a period $P = \frac{\pi}{\dot{\gamma}}\left(p + \frac{1}{p}\right)$

When particle rotations are disturbed by Brownian motion,

$D_{r0} = \frac{3k_BT(\ln(2p) - 0.5)}{\pi\eta_s L^3}$ Rotary diffusivity for a spheroid of aspect ratio p

$D_{r0} = \frac{3k_BT(\ln(L/d) - 0.8)}{\pi\eta_s L^3}$ Rotary diffusivity for rods

Non-spherical particles

Dilute suspensions of spheroids

$$\sigma = \sigma^e + \sigma^v + \sigma^s$$

$$\boldsymbol{\sigma}^e = 3\left(\frac{p^2-1}{p^2+1}\right)\nu k_B T\langle \mathbf{uu}\rangle \quad \boldsymbol{\sigma}^v = 2\eta_s\phi\left\{A\langle \mathbf{uuuu}\rangle : \mathbf{D} + B\left[\langle \mathbf{uu}\rangle \cdot \mathbf{D} + \mathbf{D}\cdot\langle \mathbf{uu}\rangle\right] + C\mathbf{D}\right\} \quad \sigma^s = 2\eta_s D$$

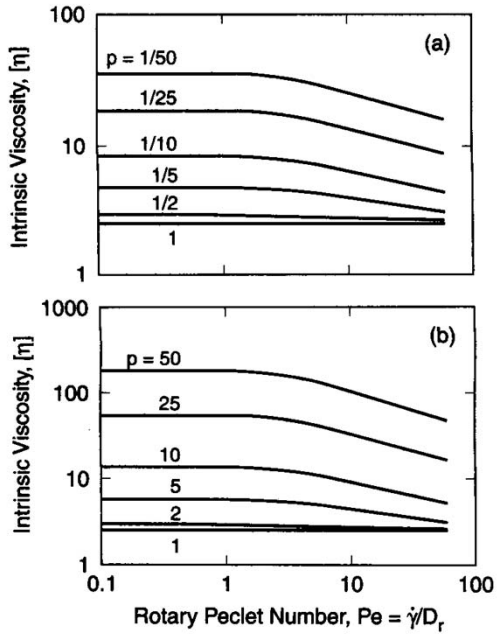

Figure 6.14 Intrinsic viscosity versus Peclet number for dilute suspensions of spheroidal particles of **(a)** oblate shape and **(b)** prolate shape. (From Macosko 1994, adapted from Brenner 1974, with permission from Pergamon Press.)

Non-spherical particles

Dilute suspensions of high-aspect-ratio particles or molecules

$$\boldsymbol{\sigma} = 2\eta_s \mathbf{D} + \nu \varsigma_{str} \langle \mathbf{uuuu} \rangle : \mathbf{D} + 3\nu k_B T \left\{ \langle \mathbf{uu} \rangle - \frac{1}{3}\boldsymbol{\delta} \right\} \qquad \varsigma_{str} = \frac{\pi \eta_s L^3}{6\ln(2L/d)} f(\varepsilon) = \frac{k_B T}{2D_{r0}}$$

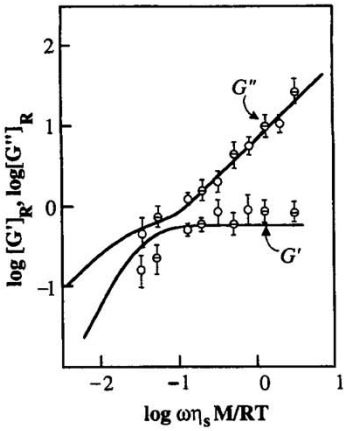

Figure 6.16 Frequency-dependence of reduced intrinsic moduli $[G']_R \equiv (5/3)\lim_{\nu\to 0} G'/\nu k_B T$; $[G'']_R \equiv (5/3)\lim_{\nu\to 0}(G'' - \omega\eta_s)/\nu k_B T$ for dilute suspensions of tobacco mosaic virus (TMV). The concentration ν is the number of particles per unit volume of solution, and is given by $\nu = cN_A/M$, where c is mass of TMV per unit volume, N_A is Avogadro's number, and M is the mass of a TMV particle. The lines are the predictions for a dilute suspension of long prolate spheroids. (From Nemoto et al., Biopolymers, 14:407, Copyright © 1975. Reprinted by permission of John Wiley & Sons, Inc.)

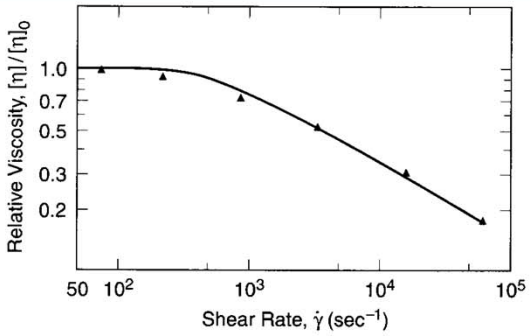

Figure 6.17 Normalized intrinsic viscosity $[\eta]/[\eta]_0$ for a dilute solution of poly(γ-benzyl-L-glutamate) (PBLG); $M_w = 208{,}000$) in *m*-cresol. The line is a calculation for the rigid-dumbbell model, with the relaxation time $\tau = 1/6D_{r0}$ adjusted to the value 10^{-3} sec to obtain a fit. The stress tensor for a suspension of rigid dumbbells is given by Eq. (6-36) with ζ_{str} replaced by $k_B T/D_{r0}$. (From Bird et al. 1987; data from Yang 1958, *Dynamics of Polymeric Liquids, Vol. 2*, Copyright © 1987. Reprinted by permission of John Wiley & Sons, Inc.)

Non-spherical particles

Semi-dilute suspensions of Brownian rods

$$\frac{\partial \psi}{\partial t} + \frac{\partial}{\partial \mathbf{u}} \cdot \left[(\mathbf{u} \cdot \nabla \mathbf{u} - \mathbf{uuu} : \mathbf{D}) \psi - \hat{D}_r \frac{\partial \psi}{\partial \mathbf{u}} \right] = 0$$

$$\boldsymbol{\sigma} = 2\eta_s \mathbf{D} + \nu \varsigma_{str} \langle \mathbf{uuuu} \rangle : \mathbf{D} + 3\nu k_B T \left\{ \langle \mathbf{uu} \rangle - \frac{1}{3} \boldsymbol{\delta} \right\}$$

$$\hat{D}_r(\mathbf{u}) = D_r \left[\frac{4}{\pi} \int |\mathbf{u} \times \mathbf{u}'| \psi(\mathbf{u}') du'^2 \right]^{-2}$$

Orientation dependent rotary diffusivity

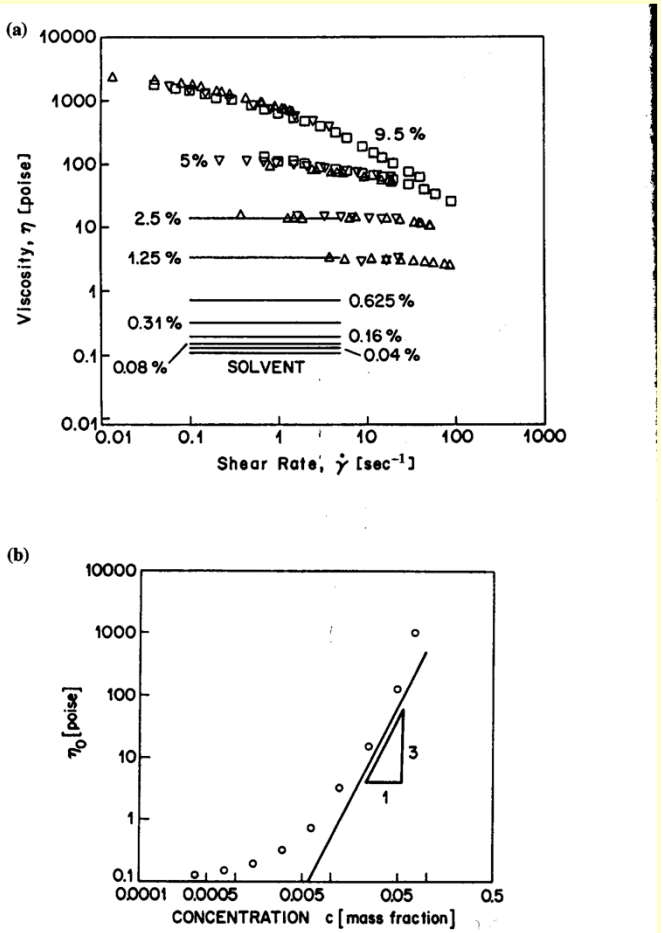

Figure 6.20 **(a)** Viscosity of solution of poly(γ-benzyl-L-glutamate) (PBLG; molecular weight 231,000), in *m*-cresol as a function of shear rate at 29°C for various mass percentages ranging from dilute ($\lesssim$0.31%) to semidilute (0.31–2.5%) to concentrated isotropic (5–9.5%). The different symbols and lines refer to data taken on different instruments. **(b)** Zero-shear viscosity as a function of concentration. (reprinted with permission from Mead and Larson, Macromolecules 23:2524. Copyright 1990 American Chemical Society.)

Non-spherical particles

Semi-dilute non-Brownian fiber suspensions

1.viscosity increase is not much
2.normal stress ~ 0.4 times shear stress $\frac{N_1}{\phi\eta_s p^{3/2}\ln(p)} = \frac{p^{5/2}C}{4}\dot{\gamma}$

3.large extensional stresses

$$\bar{\eta} = 3\eta_s + \nu\zeta_{str} = 3\eta_s\left[1+\frac{4\phi p^2}{9\ln(\pi/\phi)}\right]$$

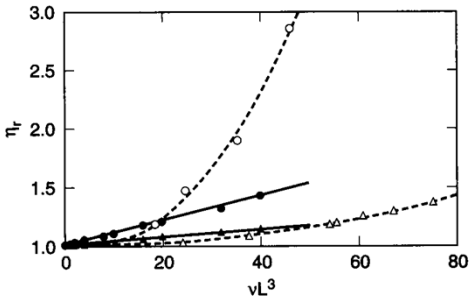

Figure 6.23 The relative viscosity at steady state of suspensions of non-Brownian rod-like particles versus dimensionless concentration νL^3. Simulations for $p \equiv L/d = 16.9$ (●), 31.9 (▲); Bibbo's (1987) experimental results for $L/d = 16.9$ (○), and 31.9 (△). (Reprinted from J Non-Newt Fluid Mech 54:405, Yamane et al. (1994), with kind permission from Elsevier Science - NL, Sara Burgerhartstraat 25, 1055 KV Amsterdam, The Netherlands.)

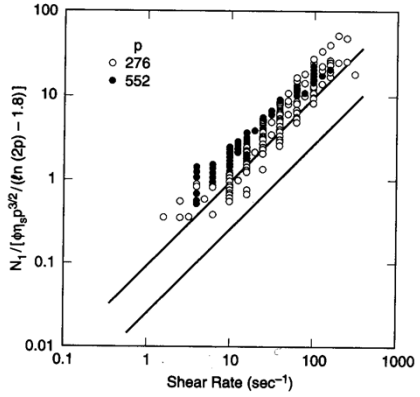

Figure 6.24 The normalized first normal stress difference $N_1/[\phi\eta_s p^3/(\ln(2p)-1.8)]$ versus shear rate for glass fibers of aspect ratios $p = 276$ and 552 in Newtonian solvents, namely, glucose wheat syrup and epoxy resin. For $p = 276$, the volume fraction ϕ is in the range 0.0002–0.0011; and for $p = 552$, $\phi = 0.00045$–0.00095. The solid lines are the upper and lower boundaries of data from Carter (1967), Kitano and Kataoka (1981), and Goto et al. (1986). (Reprinted from J Non-Newt Fluid Mech 54:153, Zirnsak et al. (1994), with kind permission from Elsevier Science - NL, Sara Burgerhartstraat 25, 1055 KV Amsterdam, The Netherlands.)

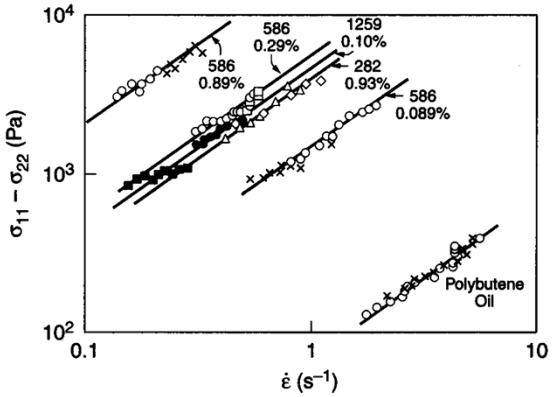

Figure 6.26 Extensional stress $\sigma_{11} - \sigma_{22}$ versus extension rate for glass fibers of aspect ratios 282, 586, and 1259 suspended in Newtonian polybutene oil (viscosity 283 P) at the volume percents shown. The straight lines have slopes of unity; the data are in excellent agreement with the equation of Batchelor (1971), Eq. (6-57). [From Macosko 1994 (adapted from Mewis and Metzner 1974), with permission from Cambridge University Press.]

Electrically charged particles

Hard spheres; coated with an organic layer that provides a steric barrier to prevent flocculation

The chages lead to long-range repulsions that can keep the particles far enough apart that they are not drawn together by short-range van der Waals forces

The surface charges increase the effective particle diameter

viscosity

at small volume fraction

$$\frac{\eta}{\eta_0} = 1 + 2.5\phi + \left[2.5 + \frac{3}{40}\left(\frac{d_{eff}}{a} \right)^5 \right] \phi^2$$

$$d_{eff} \approx \frac{1}{\kappa} \ln\{\alpha / \ln[\alpha / \ln(\alpha / \ldots)]\}$$

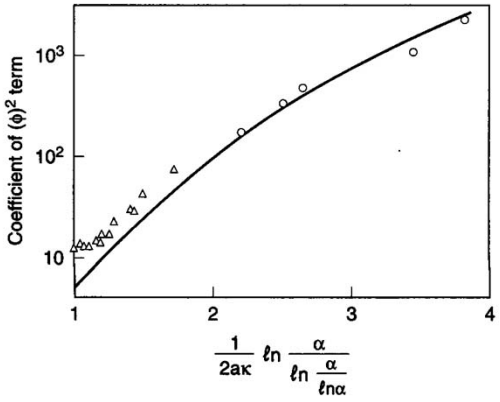

Figure 6.28 The order ϕ^2 coefficient in Eq. (6-65) for the low-shear-rate viscosity of a suspension of charged spheres of polystyrene (○) with a = 25–45 nm (Stone-Masui and Watillon 1968), and of bovine serum albumin (△) with 1 = 3.6 nm (Tanford and Buzzell 1956). The line is the prediction of Eqs. (6-65) and (6-63). (From Russel et al. 1989, with permission from Cambridge University Press.)

Electrically charged particles

viscosity

at effective volume fraction larger than 0.1 $$\frac{\eta}{\eta_s} = \left(1 - \frac{\phi_{eff}}{\phi_m}\right)^{-(5/2)\phi_m}$$

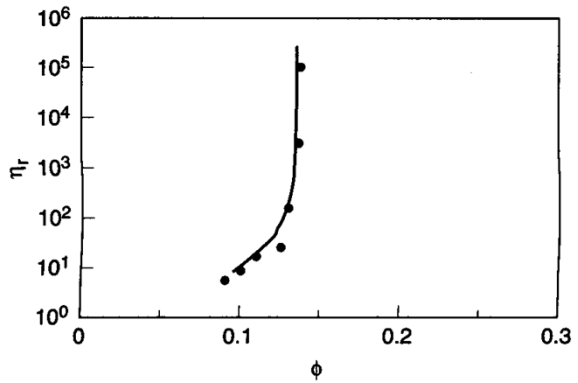

Figure 6.29 Zero-shear relative viscosity versus particle volume fraction for aqueous suspensions of charged polystyrene spheres ($a = 34$ nm) in 5×10^{-4} M NaCl (●) (Buscall et al. 1982a). The line is calculated by using Eq. (6-66) for the viscosity, with ϕ_{eff} given by Eq. (6-64), and d_{eff} by Eq. (6-67a) or (6-67b). The potential $W(R)$ is given by Eq. (6-58) or (6-59) with κ given by Eq. (6-61); the constant K is 0.10, and $|\psi_s|$ is in the range 50–90 mV. (From Buscall 1991, reproduced with permission of the Royal Society of Chemistry.)

Electrically charged particles

viscosity: shear rate dependence

as shear rate increases, hydrodynamic contribution increases, the effective particle diameter goes down, the particles approach each other more closely

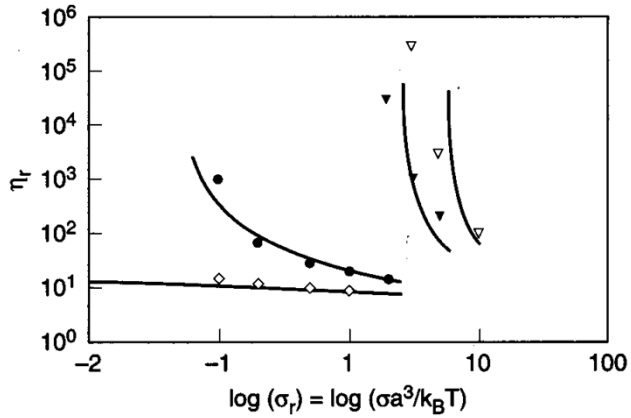

Figure 6.30 Relative viscosity versus reduced shear stress for aqueous suspensions of charged polystyrene spheres (a = 110 nm) at a concentration of ϕ = 0.40 at HCl concentrations of 0 (▽), 1.88×10^{-4} (▼), 1.88×10^{-3} (●), and 0.0188 (◇) (from Krieger and Eguiluz 1976). The solid lines are calculated using the same equations as in Fig. 6-29. (From Buscall 1991, reproduced with permission of the Royal Society of Chemistry.)

Electrically charged particles

Yield stress and modulus

The yield stress appears when the particle repulsions are strong enough to induce macrocrystallization.

As the ionic strength decreases further, the repulsions become stronger, and the yield stress becomes larger.

$$\sigma_y \approx K\left(\frac{W(r_m)-k_BT}{(r_m/2)^3}\right) \qquad r_m = 2a\left(\frac{\phi_m}{\phi}\right)^{1/3}$$

$$G'_\infty = \frac{\phi_m N}{5\pi r_m}\left\{\frac{4}{r_m}\left(\frac{dW}{dr}\right)_{r=r_m} + \left(\frac{d^2W}{dr^2}\right)_{r=r_m}\right\} \approx \frac{\phi_m N}{5\pi r_m}\kappa^2 W(r_m)$$

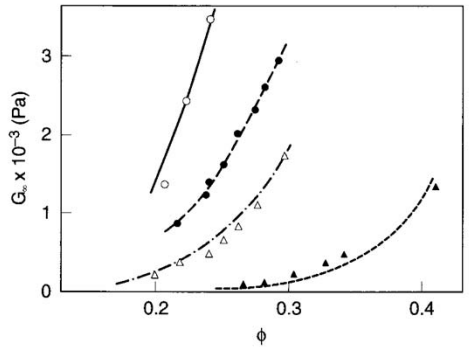

Figure 6.31 High-frequency modulus G_∞ versus particle volume fraction ϕ for charged polystyrene latices of radius $a = 26.3$ nm (◯), 34.3 nm (●), 39.2 nm (△), and 98.3 nm (▲) in aqueous solutions with 5×10^{-4} M NaCl. The lines are the predictions of the theory of Buscall et al. (1982b) for an FCC lattice with $N = 12$ and $\phi_m = 0.74$, and a best-fit value of $|\psi_s|$ increasing from 50 to 89 mV as the particle radius increases from 26.3 to 98.3 nm. These predictions differ from Eq. (6-70) only in that a prefactor (3/32) in Buscall et al. (1982b) was corrected to $1/(5\pi)$ in Buscall (1991). (From Buscall et al. 1982b, reproduced with permission of the Royal Society of Chemistry.)

Electrically charged particles

Flow mechanism
- formation of sliding layers
- breakdown of these layers as shear rate increases

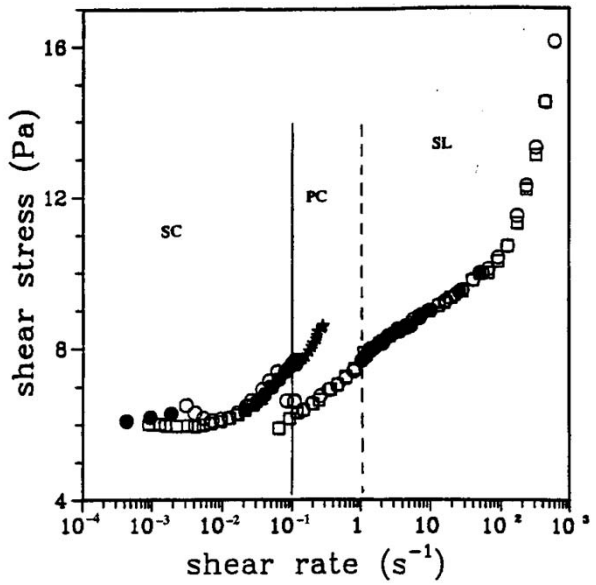

Figure 6.33 Shear stress as a function of shear rate for $a = 73$ nm charged polystyrene spheres at a volume fraction of $\phi = 0.33$ in 10^{-3} M KCl. The various symbols stand for measurements made under different conditions, namely, increasing shear rate (○), decreasing shear rate (□), constant stress (●), or metastable shear rates (∗). SC denotes the "strained-crystal" configuration shown in Fig. 6-32b, SL is the "sliding-layer" configuration in Fig. 6-32c, and PC is an intermediate "polycrystalline configuration." (From Chen et al. 1994, with permission from the Journal of Rheology.)

Electrically charged particles

Shear thinning; due to slipping of the layers past each other

Shear thickening requires not only that sliding layers be broken down by shear, but that the fragments of these layers must rotate and collide with each other to form structures whose average dimensions in the flow-gradient direction are large. Such structures can 'jam' the flow, leading to abrupt shear thickening.

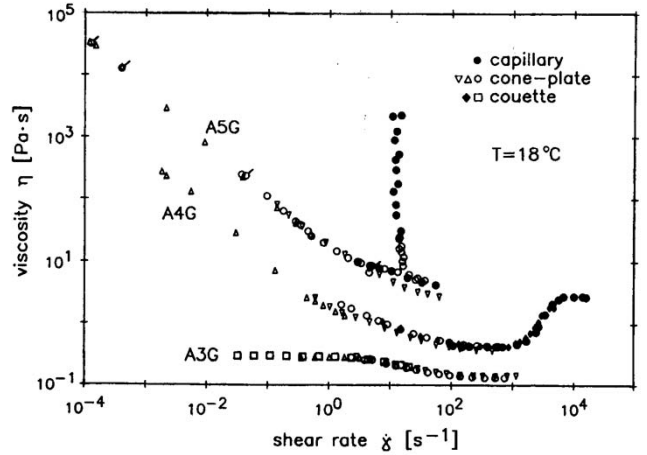

Figure 6.34 Viscosity as a function of shear rate for $a = 82.5$ nm charged particles of styrene-ethylacrylate in glycol at volume fractions ϕ of 0.523 (A5G), 0.434 (A4G), and 0.355 (A3G). (From Laun et al. 1992, with permission from the Journal of Rheology.)

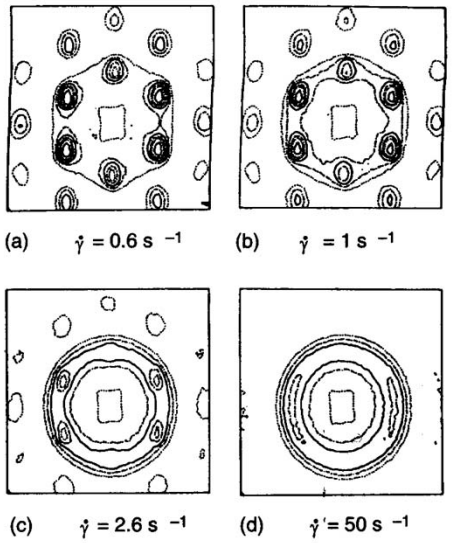

Figure 6.35 Neutron scattering patterns with the neutron beam directed in the *gradient direction* for various shear rates $\dot{\gamma}$ of suspension A4G described in the caption to Fig. 6-34. The horizontal direction is the flow direction and the vertical direction is the vorticity direction. (From Laun et al. 1992, with permission from the Journal of Rheology.)

Electrically charged particles

Normal stress difference

$$2N_2 \approx -N_1 \approx |\sigma|$$

appears only when
- LCP composed of rod-like molecules
- electrorheological suspensions which form chain-like aggregates

similarity supports the notion that in the shear thickening region, the relevant flow units are no longer spheres, but are rod-like or disk-like particle aggregates

Particles in viscoelastic liquids

- to add performance, to save cost, to potentially reduce thermal expansion stresses

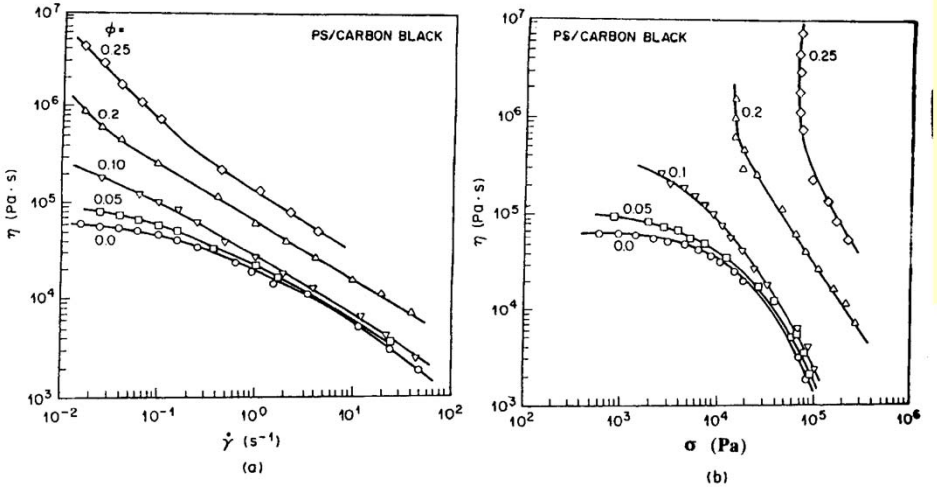

Figure 6.37 Viscosity as a function of **(a)** shear rate or **(b)** shear stress of a polystyrene melt ($M_w = 214{,}000$) filled with carbon black (surface area = 124 m²/g) at various volume fractions ϕ at 170°C. (From Lobe and White 1979, reprinted with permission from the Society of Plastics Engineers.)

effectively less elastic than polymer alone

effect of coupling agent

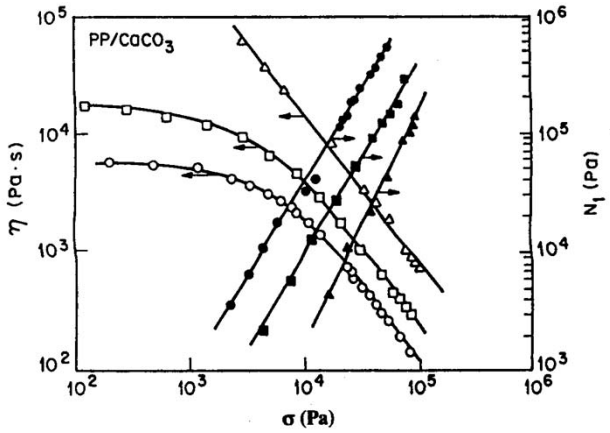

Figure 6.38 Viscosity (open symbols) and first normal stress difference (closed symbols) as a function of shear stress for neat polypropylene melt (○, ●), the same melt filled with 50% by weight $CaCO_3$ particles of size 2.5 μ, (△, ▲), and the filled melt with a titanate "coupling agent" (□, ■). (From Han et al. 1981, reprinted with permission from the Society of Plastics Engineers.)

enhanced shear thinning, because the shear rate experienced by polymer confined between two particles can be much larger than the overall shear rate

Particles in viscoelastic liquids

Thixotropy;

as the diffusion time constant is too large (order of an hour) due to high viscosity, it takes a long time for a gel-like particle structures to relax or reform, hence, flow induces changes in fluid structure that are erased only after hours of quiescence

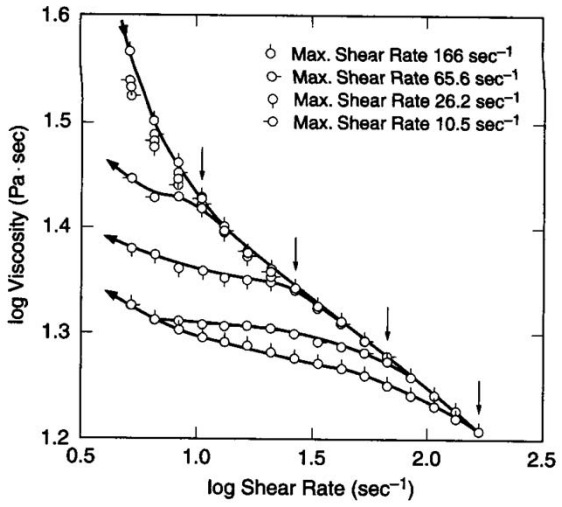

Figure 6.39 Hysteresis loops of viscosity versus shear rate of a 3% by weight suspension of fumed silica (surface area = 325 m^2/g) in poly(dimethylsiloxane), (PDMS; molecular weight = 67,000, $\eta_s \approx 125$ P) at 30°C. In each run, the shear rate was first increased up to a maximum shear rate $\dot{\gamma}_{max}$ located at the arrow, and then decreased. After a rest of 23 hours, another run was made, with a different $\dot{\gamma}_{max}$, thus producing the series of curves shown. (Reprinted from J Non-Newt Fluid Mech 17:45, Ziegelbaur and Caruthers (1985), with kind permission from Elsevier Science - NL, Sara Burgerhartstraat 25, 1055 KV Amsterdam, The Netherlands.)